FINAL TECHNICAL REPORT

NEHRP Award No. G09AP00063

Numerical Assessment Methodology for Tall Building Collapse Potential

Term Covered: June 2009 through May 2010

By Swaminathan Krishnan
California Institute of Technology,
MS 104-44, Pasadena, CA-91125, USA
Phone: (626) 395-4466 Fax: (626) 568-2719
E-mail: krishnan@caltech.edu

Numerical Assessment Methodology for Tall Building Collapse Potential – NEHRP Project Report: Award No. G09AP00063

Swaminathan Krishnan[1]

ABSTRACT

We parameterize ground motion velocity waveforms using triangular wave trains with a characteristic period, amplitude, and duration (number of cycles). We perform a suite of analyses of four tall building models subjected to these idealized wave trains, with periods (T) varying from 0.5s to 6.0s, amplitude (PGV) varying from 0.125 m.s^{-1} to 2.5 m.s^{-1}, and varying number (N) of cycles (1–5, 10). We create databases of peak transient interstory drift ratio (IDR) for each model. We show that for near-source records and synthetic waveforms from large earthquakes in the Los Angeles basin, the structural response can be rapidly estimated by determining the best-fit to one of the idealized wave-trains for which the structural responses are readily available in the databases. To assess the sensitivity of structural response to various ground motion features, we create maps of structural response in the T-PGV and PGD-PGV planes for each N. The collapse region is shown to occur only in the long-period large-amplitude regime. The region expands to lower periods and lower amplitudes with increasing ground motion cycles.

INTRODUCTION

There are two key objectives of this study:

(i) To develop a rapid estimation procedure for tall building earthquake damage.

(ii) To determine the sensitivity of the collapse regime of tall building response to three ground motion features, frequency content, intensity, and duration.

To achieve these objectives, an appropriate simplified (idealized) representation of the ground motion waveform is required. The parameters of the idealized waveforms can then be varied to gain an understanding of response sensitivity. Likewise, a small finite parameter set will allow the creation of a database of structural responses for various combinations of these parameters. For swift post-earthquake response, this database can be used for rapid estimation of tall building damage at locations where records become available immediately

[1]California Institute of Technology, MS 104-44, Pasadena, CA-91125, USA; E-mail: krishnan@caltech.edu

following an earthquake. The rapid damage estimation can be extended to an entire region by combining the procedure with the near real time earthquake simulations from a portal such as http://shakemovie.caltech.edu.

The idealized representation of the ground motion must be such that the response of tall buildings under the true waveforms is very similar to that under their idealized representations. Here, we focus on two tall steel moment frame buildings and their variants.

Building 1 is an existing 18-story office building, located within five miles of the epicenter of the 1994 Northridge earthquake. An isometric view of its FRAME3D model is shown in Figure 1(a). It was designed according to the 1982 UBC and completed in 1986-87. The height of the building above ground is 75.7 m (248' 4") with a typical story height of 3.96 m (13' 0") and taller first, seventeenth, and penthouse stories. The lateral force-resisting system consists of two-bay welded steel moment-frames, two apiece in either principal direction of the structure as shown in Figure 1(c). The location of the north frame one bay inside of the perimeter gives rise to some torsional eccentricity. Many moment-frame beam-column connections in the building fractured during the Northridge earthquake, and the building has been extensively investigated since then by engineering research groups (SAC 1995). Fundamental periods, computed assuming 100% dead load and 30% live load contribution to the mass, are 4.52s (X-translation), 4.26s (Y-translation) and 2.69s (torsion). We consider two models of Building 1, one with connections susceptible to fracture, and the other with perfect connections. Two orthogonal orientations (with respect to the strong component of the ground motion) are considered for the model with perfect connections.

Building 2, a FRAME3D model of which is shown in Figure 1(b), is similar to Building 1, but the lateral force-resisting system has been redesigned according to the 1997 UBC. It has been designed for larger earthquake forces and greater redundancy in the lateral force-resisting system, with 8 bays of moment-frames in either direction (although lateral resistance will likely be dominated by the three-bay moment frames shown in Figure 1(d) as opposed to the single-bay moment frames). The frame located in the interior of Building 1 has been relocated to the exterior, eliminating the torsional eccentricity. Fundamental periods, computed assuming 100% dead load and 30% live load contribution to the mass, are 4.06s (X-translation), 3.85s (Y-translation) and 2.60s (torsion). Detailed floor plans, beam and column sizes, and the gravity, wind and seismic loading criteria for Buildings 1 and 2 can be found in (Krishnan, Ji, Komatitsch, and Tromp 2005) and (Krishnan, Ji, Komatitsch, and Tromp 2006a). Only one variant of Building 2 is modeled here, that with perfect connections.

Consider the ground motion idealization shown in Figure 2. Although a single cycle is shown there, we consider multiple cycles with identical period and amplitude to effectively represent long duration ground motions. Thus, three parameters are used to characterize the ground velocity waveform, period T, amplitude V,

and number of cycles N. Using the Least Absolute Deviation method (L_1 norm), we determine the best fitting single-cycle idealized waveform to the strong component of 18 near-source records (velocity waveforms) from the Cape Mendocino, Chi-Chi, Imperial Valley, Iran, Kobe, Loma Prieta, Landers, Northridge, San Fernando, and Superstition Hills earthquakes. These fits are shown in Figures 3 through 5 (best-fitting 2-, 3-, 4-, 5-, and 10-cycle waveforms are shown as well, although these are not utilized in the forthcoming analysis since all the records have a prominent near-source pulse that is likely to dominate the structural response). The reason for using velocity waveforms for the curve-fitting is two-fold. First, velocity waveforms typically do not have static offsets and they are of sufficiently low frequency for the convenient identification of cycles. Second, structural damage is known to be best correlated with PGV and using PGV as the intensity parameter in the ground motion characterization would be beneficial to the damage estimation procedure.

The FRAME3D models of Building 1 (susceptible connections) and Building 2 (perfect connections) are analyzed under the 18 three-component near-source records. The peak transient interstory drift ratio (IDR) which can be considered to be the peak instantaneous tilt in a story normalized by its height is used as a measure of structural performance. The same models are also analyzed under the one-component best-fitting single-cycle idealized waveforms. Shown in Figures 6 and 7 is the comparison of the profiles of peak IDR over the height under the actual and idealized motions for the two models. The consistently good match of the profiles indicates that the particular idealization adopted here to characterize the ground motion can be very effectively used in estimating tall building response. The peak values of IDR from the two sets of analysis are compared against each other and the errors are quantified in Figure 8. The IDR errors have a Gaussian mean of 0.00056 and standard deviation of 0.0069.

Given that the response under the suitably parameterized idealized surrogate waveforms closely resembles that under the actual waveforms, it is now useful to generate a database of structural responses for all realistic combinations of surrogate waveform parameters. When recorded waveforms at various locations become available after an earthquake, the closest surrogate to each of the recorded waveforms can be determined. For swift disaster response, the damage to tall buildings at these locations can then be rapidly estimated using a table look-up approach. With this goal in mind, we have analyzed the two building models and their variants under idealized single-component waveforms with period varying between 0.5s and 6.0s at 0.25s intervals, PGV varying between 0.125 $m.s^{-1}$ 2.5 $m.s^{-1}$, and the number of cycles ranging from 1 to 5. Four databases have been created corresponding to (a) Building 1 (susceptible connections) under X direction excitation, (b) Building 1 (perfect connections) under X direction excitation, (c) Building 1 (perfect connections) under Y direction excitation, and (d) Building 2 (perfect connections) under X direction excitation. We test the veracity of the rapid

estimation approach on our 1857-like San Andreas earthquake simulation (Krishnan et al. 2006a; Krishnan et al. 2006b).

1857-LIKE SAN ANDREAS EARTHQUAKE: TALL BUILDING RESPONSE ESTIMATION

On January 9, 1857, a large earthquake of magnitude 7.9 occurred on the San Andreas fault, with rupture initiating at Parkfield in Central California and propagating in a southeasterly direction over a distance of more than 360 km. Such a unilateral rupture produces significant directivity toward the San Fernando and Los Angeles basins. Indeed, newspaper reports of sloshing observed in the Los Angeles river point to long-duration (1–2 min) and long-period (2–8 s) shaking. If such an earthquake were to happen today, it could impose significant seismic demand on present-day tall buildings. In 2005-06, using state-of-the-art computational tools in seismology and structural engineering, validated using data from the January 17, 1994, magnitude 6.7 Northridge earthquake, we simulated the damage to Buildings 1 (susceptible connections) and 2 (perfect connections) at 636 sites in southern California due to ground motion from an 1857-like hypothetical magnitude 7.9 earthquake on the San Andreas fault (Krishnan et al. 2006a; Krishnan et al. 2006b). Our study indicated that serious damage occurs in these buildings at many locations in the region in the north-to-south rupture scenario. The peak velocity simulated was of the order of 1 $m.s^{-1}$ in the Los Angeles basin, including downtown Los Angeles, and 2 $m.s^{-1}$ in the San Fernando valley, while the peak displacements were of the order of 1 m and 2 m in the Los Angeles basin and San Fernando valley, respectively. Whereas the east component is the stronger component at many locations (e.g., West Los Angeles; see Figure 9), the north component is stronger at some locations (e.g., Downey).

Here, we analyze the Building 1 (perfect connections) model under the 636 three-component synthetic motions (lowpass-filtered at a corner at 2s). The building's X direction is oriented in the geographical east direction. The peak transient IDR at all the locations is shown on a regional map in Figure 10(a). To see whether we could have rapidly estimated this regional damage map, we first determine the best-fit 1-, 2-, 3-, 4-, and 5-cycle surrogate idealized waveforms (five idealized representations) for the two horizontal components of the 636 three-component ground motion histories. The L1 norm (least absolute deviation) is used for this optimization. In the first attempt, we determine from the structural response database, the peak transient IDR at each location in either direction as the maximum of that under each of the five best-fit 1-, 2-, 3-, 4-, and 5-cycle waveforms. For the east component idealization, the database corresponding to Building 1 (perfect connections, excitation in X direction) is used. For the north component idealization, the database corresponding to Building 1 (perfect connections, excitation in Y direction) is used. Typical buildings are provided with lateral force-resisting systems in two mutually orthogonal directions to counter the two horizontal components of ground

shaking. For rapid estimation purposes, the responses in the two directions are assumed to be independent. Inherent in this estimation procedure is that torsion does not play a serious role in dictating structural response. Even for perfectly symmetric buildings, this assumption may not be valid due to asymmetric yielding, especially when approaching the collapse regime. However, it may be a fairly reasonable assumption to arrive at ball-park predictions. This first attempt in response estimation resulted in under-estimation in certain locations where there was one big pulse followed by a trailing wave-train with somewhat lower amplitudes. The best-fit single cycle idealization captures the first peak well, but misses out on the trailing wave train, whose effects are then left out resulting in response under-estimation. The best-fit multi-cycle idealization has an amplitude that is closer to the trailing wave train's amplitude. As a result, the effect of the strong first peak is not captured, once again resulting in under-estimation. To account for these special cases, we modify the approach slightly as follows:

(i) Determine the best-fitting 1-, 2-, 3-, 4-, and 5-cycle waveforms to the two horizontal components of the measured or synthetic record.

(ii) Query the structure response database for the peak transient IDR under each of the ten idealized waveforms (1–5 cycles and two components), with due consideration to the building orientation relative to the azimuth of the two ground motion components. In the San Andreas example, the X direction database is used to estimate the peak IDR under the east component idealizations, while the Y direction database is used for IDR estimation under the north component idealizations. The peak IDR is the maximum of the 10 IDRs resulting from the database queries, except for cases where the PGV of the I-cycle idealization differs from that of the J-cycle idealization by 0.25 m.s^{-1} or 0.375 m.s^{-1}, with J varying from 1 to I-1.

(iii) Consider the case where the 3-cycle idealization has an amplitude of 1.25 m.s^{-1}, while the 1-cycle idealization has an amplitude of 1.625 m.s^{-1} (the amplitudes differ by a moderate 0.375 m.s^{-1}). Furthermore, let the location of peak IDR under the 3-cycle idealization match that under the 1-cycle idealization. In this case, we assume that the entire IDR from the first strong cycle is permanent (plastic) in nature. It follows that the peak IDR under the 3-cycle idealization is the IDR from the first strong cycle plus the IDR under a 2-cycle idealization (for the trailing two cycles) whose amplitude is slightly smaller than the amplitude of the original 3-cycle idealization. The corrected velocity amplitude for the trailing 2-cycle idealization is given by: $V_I^{corr} = \frac{I*V_I - J*V_J}{I-J}$. This correction eliminates the contribution of the first strong pulse to the amplitude of the original 3-cycle idealization. Using the amplitude of the original 3-cycle idealization in estimating the IDR under the trailing 2-cycle wave would overestimate the total IDR.

The pseudocode for the rapid damage estimation procedure is outlined in Figure 11. The peak transient

IDR response of Building 1 (perfect connections) under the synthetic ground motion from the 1857-like San Andreas at each of the 636 analysis sites is estimated using this procedure. The results are shown in Figure 10(b) for convenient comparison against the actual values shown in Figure 10(a). The actual and estimated values for all analysis sites are sown plotted against each other in Figures 12(a) and 12(b). The errors are also quantified in the histogram and its best-fit Gaussian distribution in Figure 12(c). They have a Gaussian mean of 0.0011 and standard deviation of 0.021 which is somewhat high. To understand the effectiveness of the rapid estimation procedure, the IDRs must be related to useful damage measures or performance levels which can be used in the decision-making process for disaster response. Unfortunately, there is sparse data in this regard and empirical methods must be resorted to. One such method is outlined by the Federal Emergency Management Agency (FEMA 2000) which relates peak IDR directly to the following performance levels: Immediate Occupancy (IO), where very limited structural damage has occurred; Life Safety (LS), a damage state that includes damage to structural components but retains a finite margin against collapse; and Collapse Prevention (CP), a damage state at which the structure continues to support gravity loads but retains no margin against collapse. For existing buildings, the interstory drift ratio (IDR) limits for the IO, LS, and CP performance levels specified by FEMA are 0.007, 0.025, and 0.05, respectively. These numbers were not intended to be hard criteria upon which performance would be judged. Nevertheless, in the absence of other criteria, they provide a basis for performance assessment. In addition to these criteria, it is of interest to determine whether a building would be red-tagged. In thousands of collapse analyses conducted by the authors on models such as the ones considered in this study, a large percentage of models lose stability beyond peak IDRs of 0.10. Given that the models do not include certain critical failure modes such as local buckling in column flanges, the peak IDR range of 0.075-0.100 (CO) may be indicative of complete collapse (unstable). Models with intermediate peak IDRs in the range of 0.050-0.075 are assumed to be on the verge of collapse (neutrally stable) and hence may have to be red-tagged (RT). From this description, it is clear that the standard deviation of the rapid damage estimation procedure is roughly equivalent to one performance level. In other words, estimated IDR with an error of one-σ will be off the mark by one performance level, for instance, if the true performance level is RT, the prediction may be either CP or CO. Of course, on the average, the rapid estimation procedure performs rather well. Shown in Figure 12(d) are the fragilities for each of the performance levels (cumulative probability of exceedance of a given performance level as a function of PGV), computed using the actual and estimated IDRs. The IO, LS and CP fragilities derived using estimated IDRs agree very well with those derived using actual IDRs, with probability of exceedance not differing by more that 3%. The estimation procedure over-predicts the probability of exceedance of the RT and CO performance levels by up to 10%.

Finally, the estimation of IDR under the near-source records described earlier is revisited using the mod-

ified rapid damage estimation procedure adopted for the San Andreas study. The results are summarized in Figure 13. The error in IDR now has a Gaussian mean of -0.0014 and a standard deviation of 0.0086, both being marginally worse than the original estimation procedure. It may be prudent to classify records as near-source or otherwise prior to adopting one estimation procedure or the other.

TALL BUILDING RESPONSE SENSITIVITY TO GROUND MOTION FEATURES

A useful by-product of the rapid damage estimation study is the sensitivity of tall building response to the ground motion parameters of period (T), intensity (PGV), and duration (as measured by the number of cycles N) that can be extracted from the databases of structural response under the idealized wave excitation. The relationship between the ground excitation and its effects on structures can be conveniently displayed in color maps/contours of peak IDR on the T-PGV plane (or the PGD-PGV plane), one map for each N (Figures 14 and 15 for Building 1 (susceptible connections) under X direction excitation, Figures 16 and 17 for Building 1 (perfect connections) under X direction excitation, Figures 18 and 19 for Building 1 (perfect connections) under Y direction excitation, and Figures 20 and 21 for Building 2 (perfect connections) under X direction excitation). Also shown on these maps are the story locations where these peak values occur. The threshold values of (a) idealized wave period at PGV of 2.5m.s^{-1} and (b) PGV at period of 6s, at various number of idealized wave cycles, for the exceedance of the CP, RT, and CO performance levels are listed in Table 1 for all four building models. The following observations can be made:

(i) The threshold PGV and period for each performance level falls with increasing number of ground motion cycles. These drops are not continuous or proportional.

(ii) CO performance level is exceeded only under long period ground motion, with the period being relative to the fundamental natural period of the building. For instance, Building 1 has a fundamental period of 4.52s. Under ground motion with 3 strong cycles or fewer, the CO performance can be exceeded only if the idealized waveform has a period of 4.5s or longer. Building 2 has a fundamental period of 4.05s and exceeding the CO performance level requires a 3-cycle waveform with period of at least 3.25s.

(iii) Building 2 is stronger than Building 1 by about 20% (as measured using a simple pushover analysis) and is significantly stiffer. In general, a higher PGV (0.125–0.25m.s^{-1}) is required for the CO performance level to be exceeded when compared against Building 1, although it is susceptible to shorter period ground motion than Building 1.

(iv) Thresholds of 4.5s and 1.625m.s^{-1} can be inferred for the excitation period and PGV, respectively, for

Model	N	Thresholds for CP		Thresholds for RT		Thresholds for CO	
		PGV @ T=6s	T @ PGV=2.5m.s^{-1}	PGV @ T=6s	T @ PGV=2.5m.s^{-1}	PGV @ T=6s	T @ PGV=2.5m.s^{-1}
B–1	1	0.750	2.00	1.125	3.75	1.625	4.50
(susceptible)	2	0.625	1.75	0.750	3.75	0.875	4.50
X direction	3	0.625	1.50	0.750	3.50	0.750	4.50
excitation	4	0.500	1.50	0.625	2.25	0.625	4.00
	5	0.625	1.25	0.625	2.25	0.625	2.50
B–1	1	0.750	2.00	1.250	4.50	1.875	5.50
(perfect)	2	0.750	2.00	0.875	4.50	1.125	5.00
X direction	3	0.625	2.00	0.750	4.25	0.875	4.75
excitation	4	0.625	2.00	0.750	4.00	0.750	4.50
	5	0.625	2.00	0.625	3.50	0.750	4.25
B–1	1	0.875	1.75	1.125	4.50	1.625	5.25
(perfect)	2	0.750	1.75	0.875	4.50	1.000	4.75
Y direction	3	0.625	1.75	0.750	4.25	0.875	4.50
excitation	4	0.625	1.75	0.750	3.50	0.750	4.25
	5	0.625	1.50	0.625	2.25	0.625	3.25
B–2	1	1.125	2.75	1.500	3.75	1.875	4.50
(perfect)	2	0.875	2.25	1.125	3.25	1.375	3.75
X direction	3	0.875	2.00	1.000	2.75	1.125	3.25
excitation	4	0.875	2.00	0.875	2.50	1.000	2.75
	5	0.750	2.00	0.875	2.25	0.875	2.50

Table 1: Peak ground velocity and period thresholds for the exceedance of the CP, RT, and CO performance levels for all building models. N is the number of cycles of ground excitation.

collapse to definitively occur under one-cycle excitation (i.e., near-source ground motion). The corresponding numbers for red-tagging are 3.75s and 1.125m.s^{-1}, respectively. These thresholds drop with increasing number of ground motion cycles. For three-cycle excitation, the collapse thresholds are 3.25s and 0.75m.s^{-1}, respectively, and red-tagging thresholds are 2.75s and 0.75m.s^{-1}, respectively.

(v) Under multi-cycle long period ground motion, there is little difference in PGV thresholds for CP, RT, and CO performance levels. This points to a dichotomy in performance, with performance being satisfactory if the threshold is not exceeded, and catastrophic collapse occurring otherwise.

CONCLUSIONS

An efficient rapid damage estimation procedure has been developed. It involves analyzing structural models under a suite of idealized ground motion waveforms characterized by a period, an amplitude, and a duration represented by the number of cycles. The analyses are performed with excitation applied in either direction and the results are stored in a database. For the estimation of structural response under a measured ground motion record, the idealized waveforms that have the least absolute deviation from the two horizontal components of the record are determined. Structural responses are rapidly estimated by querying the database. A modified approach is necessary to account for special cases involving one big pulse, followed by several moderate pulses. The response database provides us insights into the sensitivity of ground motion features on the response of tall buildings. Near-source ground motion with pulse-periods longer than 4.5s and PGV greater than 1.625m.s^{-1}, and 3-cycle motion with cycle-periods longer than 3.25s and PGV greater than 0.75m.s^{-1} causes collapse in the 18-story steel moment frame buildings considered in this study.

REFERENCES

FEMA (2000). *Prestandard and Commentary for the Seismic Rehabilitation of Buildings*. FEMA-356. Federal Emergency Management Agency, USA.

Krishnan, S., C. Ji, D. Komatitsch, and J. Tromp (2005). Performance of 18-story steel moment frame buildings during a large San Andreas earthquake – a Southern California-wide end-to-end simulation. Technical Report EERL 2005-01, http://caltecheerl.library.caltech.edu, Earthquake Engineering Research Laboratory, California Institute of Technology, Pasadena, California, USA.

Krishnan, S., C. Ji, D. Komatitsch, and J. Tromp (2006a). Case studies of damage to tall steel moment frame buildings in southern California during large San Andreas earthquakes. *Bulletin of the Seismological Society of America 96*(4), 1523–1537.

Krishnan, S., C. Ji, D. Komatitsch, and J. Tromp (2006b). Performance of two 18-story steel moment frame buildings in southern California during two large simulated San Andreas earthquakes. *Earthquake Spectra 22*(4), 1035–1061.

SAC (1995). Analytical and field investigations of buildings affected by the Northridge earthquake of January 17, 1994 – Part 1. Technical Report SAC 95-04, Part 1, Structural Engineers Association of California, Applied Technology Council, and California Universities for Research in Earthquake Engineering, USA.

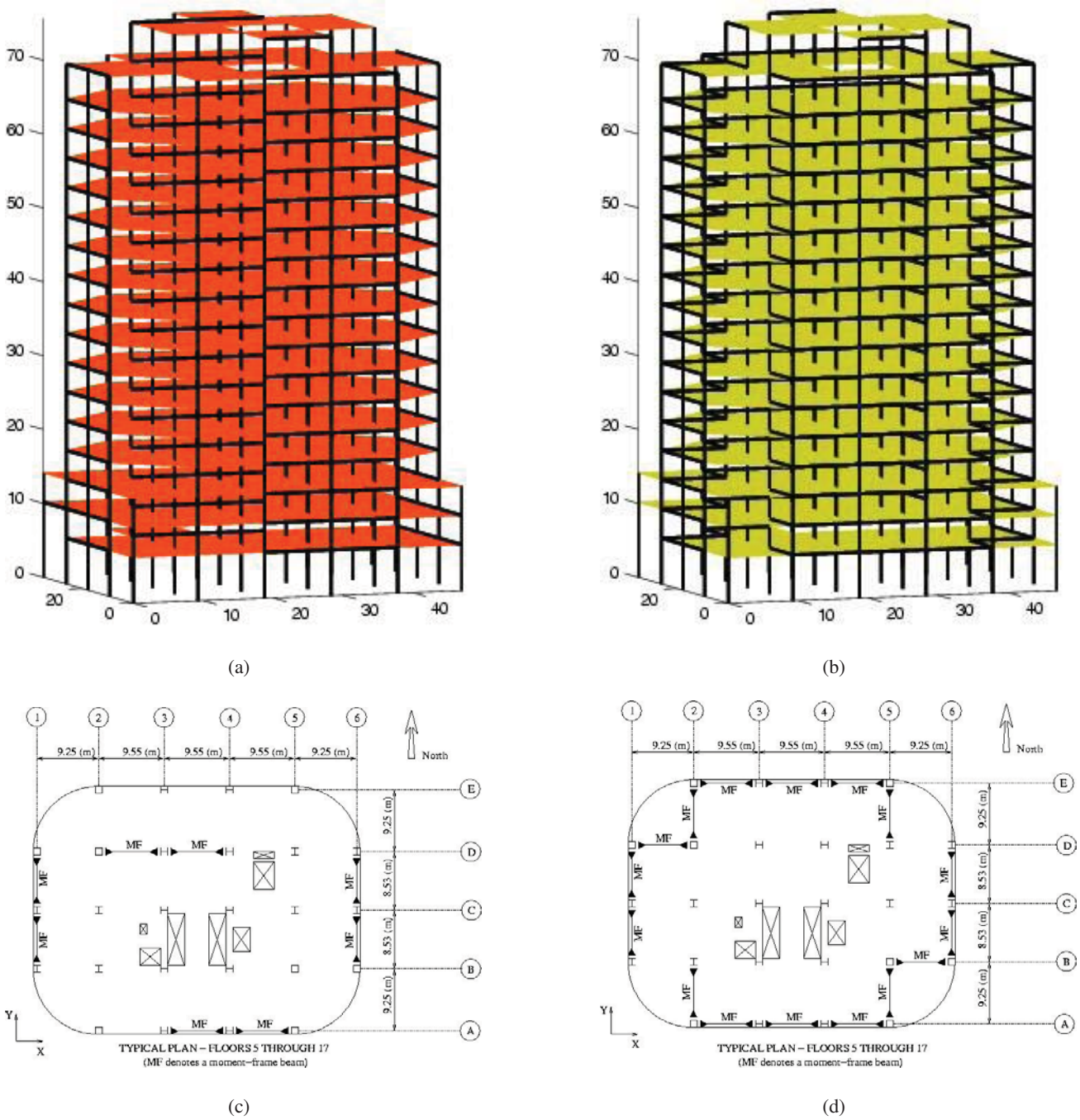

Figure 1: Structural models of the two 18-story steel moment frame buildings: (A) Isometric view of the existing building (designed using the 1982 UBC). (B) Isometric view of the new building (redesigned using the 1997 UBC). (C) Plan view of a typical floor of the existing building showing the location of columns and moment-frame (MF) beams. (D) Plan view of a typical floor of the redesigned building.

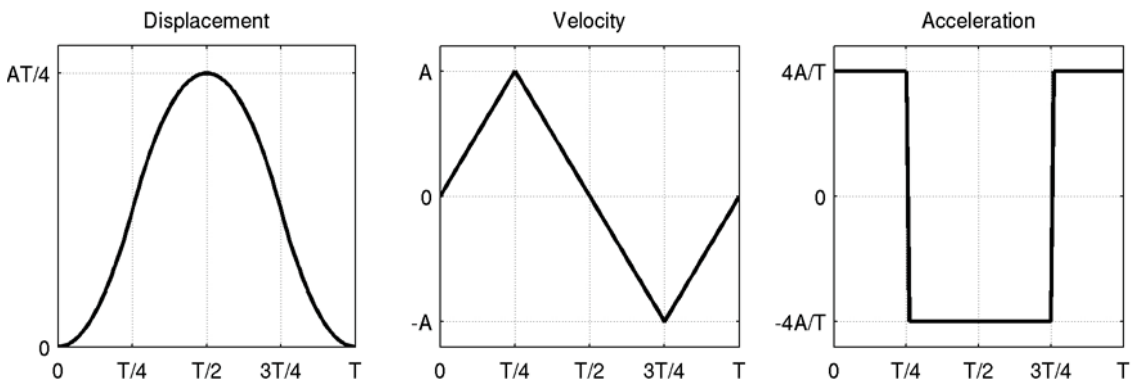

(a) (b) (c)

Figure 2: Waveforms for the (a) displacement, (b) velocity, and (c) acceleration of the idealized pulses used as input ground motions.

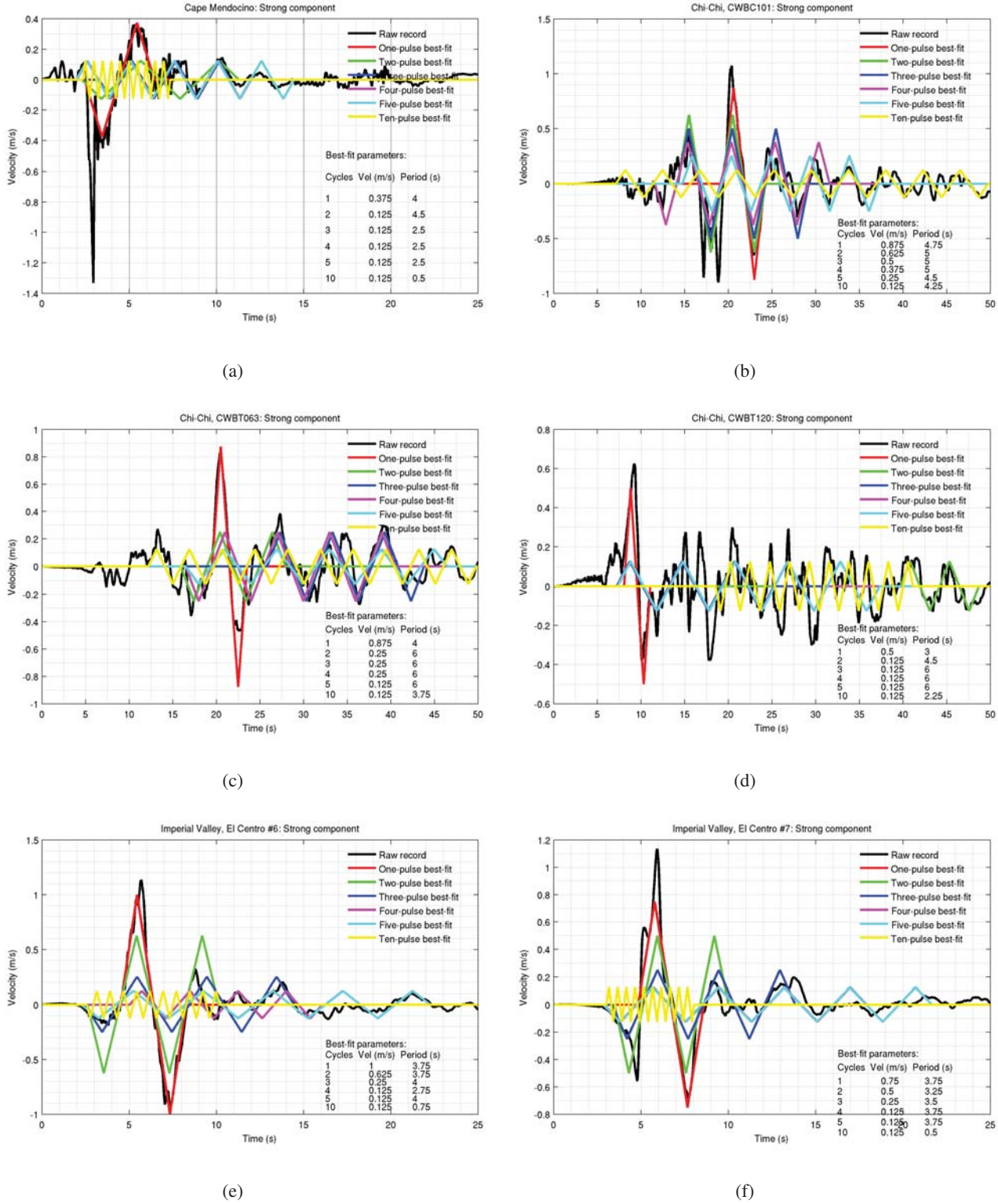

Figure 3: Near-source ground motion records from the Cape Mendocino, Chi-Chi, and Imperial Valley earthquakes. Also shown are the idealized 1-, 2-, 3-, 4-, 5-, and 10-cycle wave trains with the least absolute deviation (L1 norm) from the corresponding record.

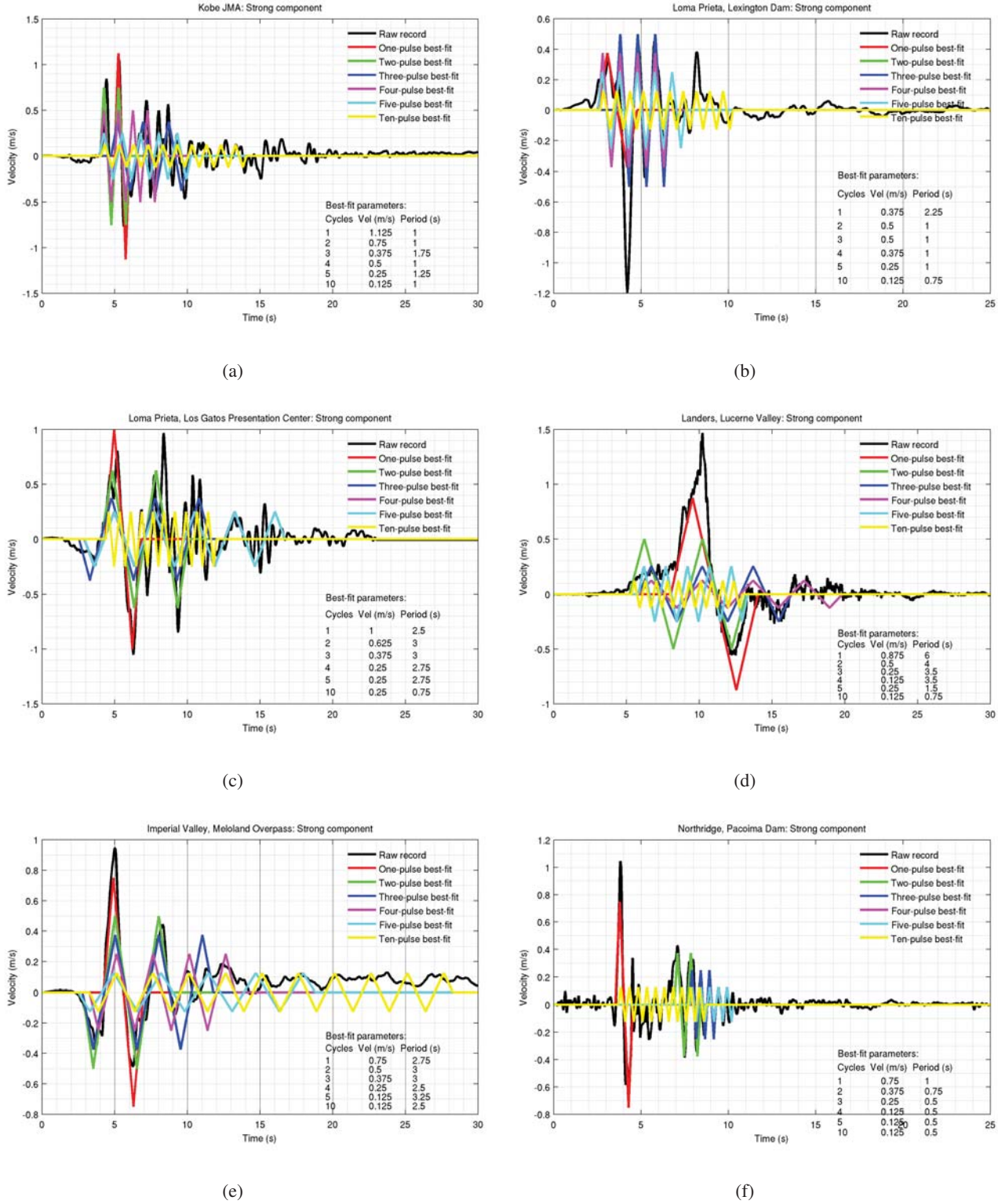

Figure 4: Near-source ground motion records from the Kobe, Loma Prieta, Landers, Imperial Valley, and Northridge earthquakes. Also shown are the idealized 1-, 2-, 3-, 4-, 5-, and 10-cycle wave trains with the least absolute deviation (L1 norm) from the corresponding record.

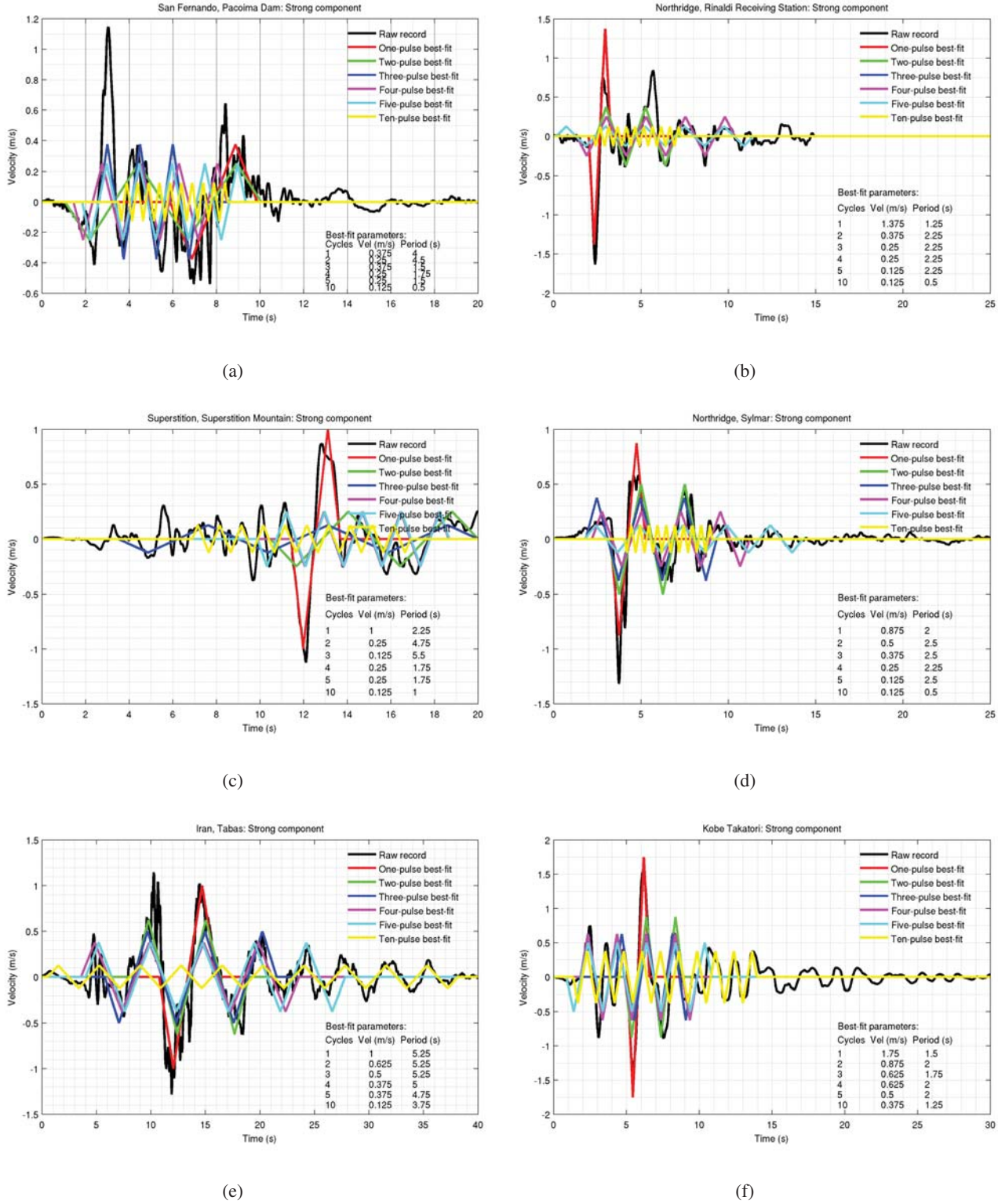

Figure 5: Near-source ground motion records from the San Fernando, Northridge, Superstition, Iran, and Kobe earthquakes. Also shown are the idealized 1-, 2-, 3-, 4-, 5-, and 10-cycle wave trains with the least absolute deviation (L1 norm) from the corresponding record.

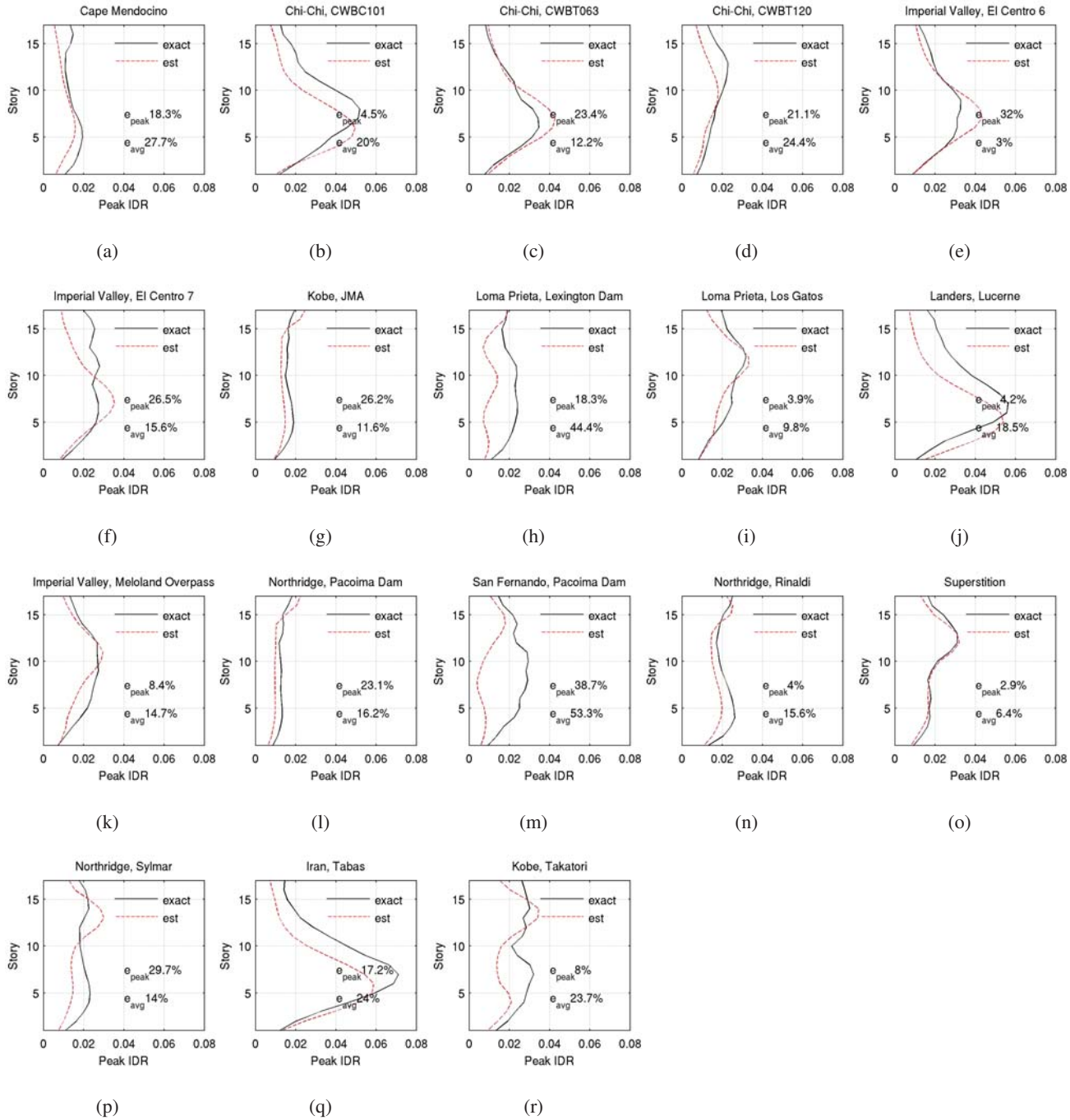

Figure 6: Comparison of peak transient IDR profile over building height computed using real record against that computed using the best-fit idealized 1-cycle wave: Building 1 (susceptible connections).

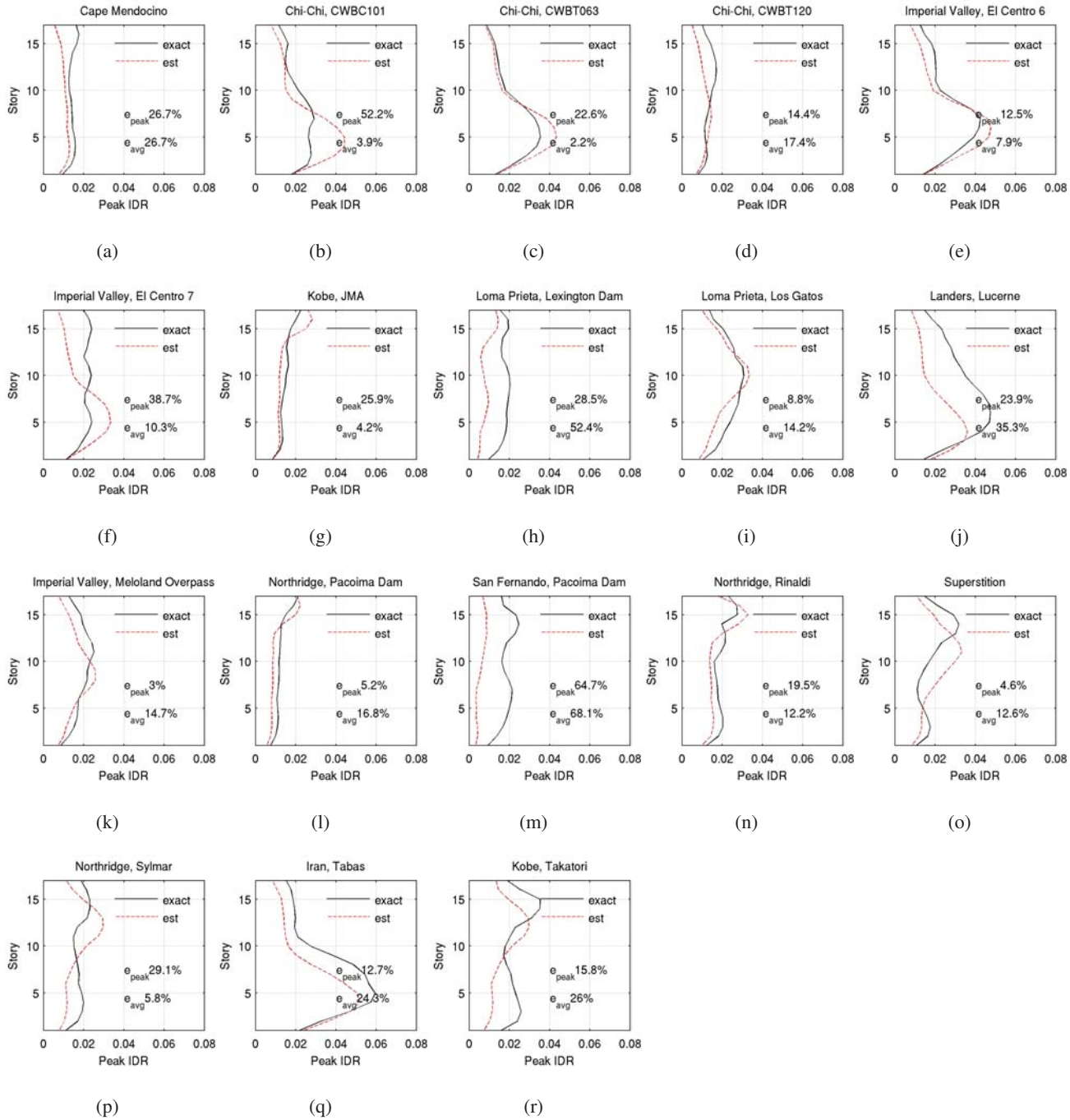

Figure 7: Comparison of peak transient IDR profile over building height computed using real record against that computed using the best-fit idealized 1-cycle wave: Building 2 (perfect connections).

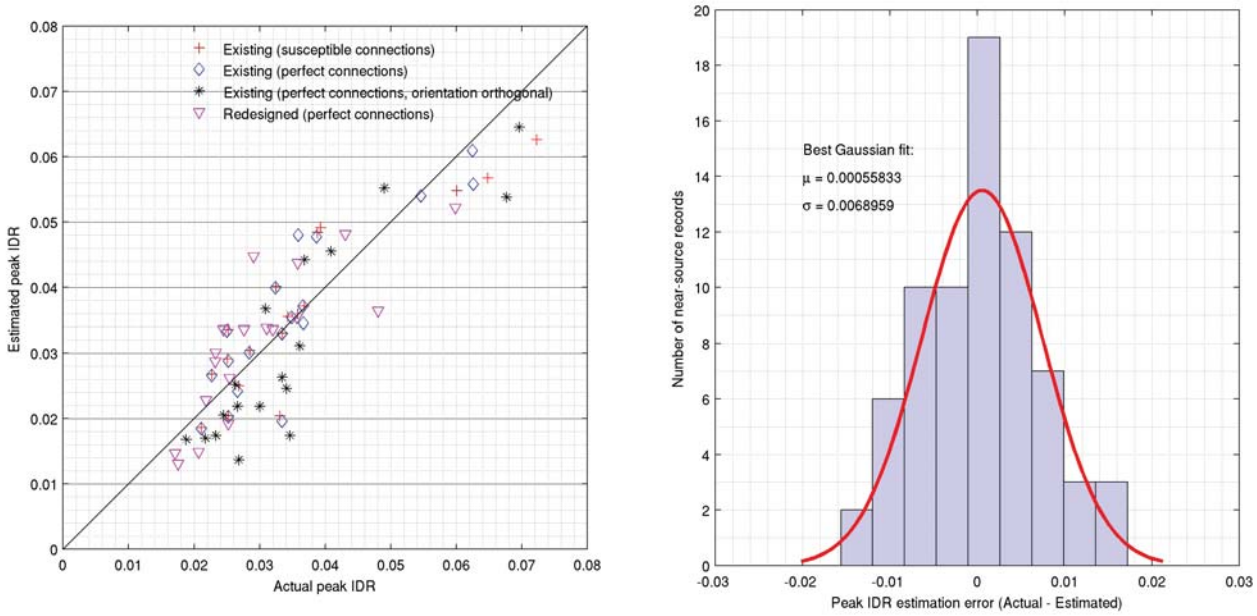

(a) (b)

Figure 8: (a) Peak transient IDR computed using all near-source records plotted against that computed using best-fit idealized 1-cycle waves: All buildings. The diagonal line represents identical results from the two analyses. (b) Histogram of the error in determining the peak transient IDR from the idealized waveform as opposed to the actual record. The best-fit Gaussian is also shown.

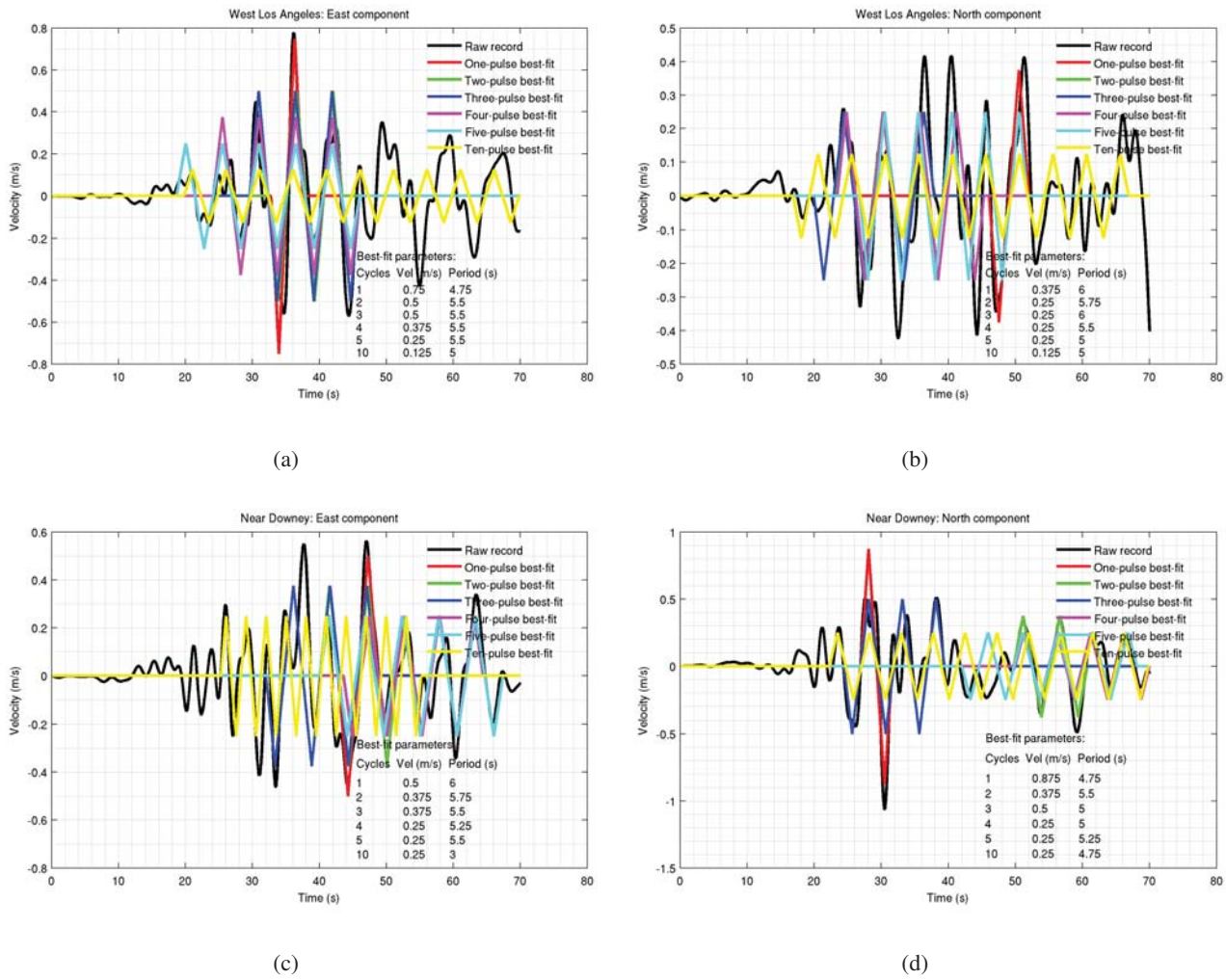

Figure 9: Synthetic velocity waveforms at sites in West Los Angeles [(a) east component; (b) north component] and Downey [(c) east component; (d) north component] from a simulated 1857-like San Andreas fault earthquake. Also shown are the idealized 1-, 2-, 3-, 4-, 5-, and 10-cycle wave trains with the least absolute deviation (L1 norm) from the corresponding record.

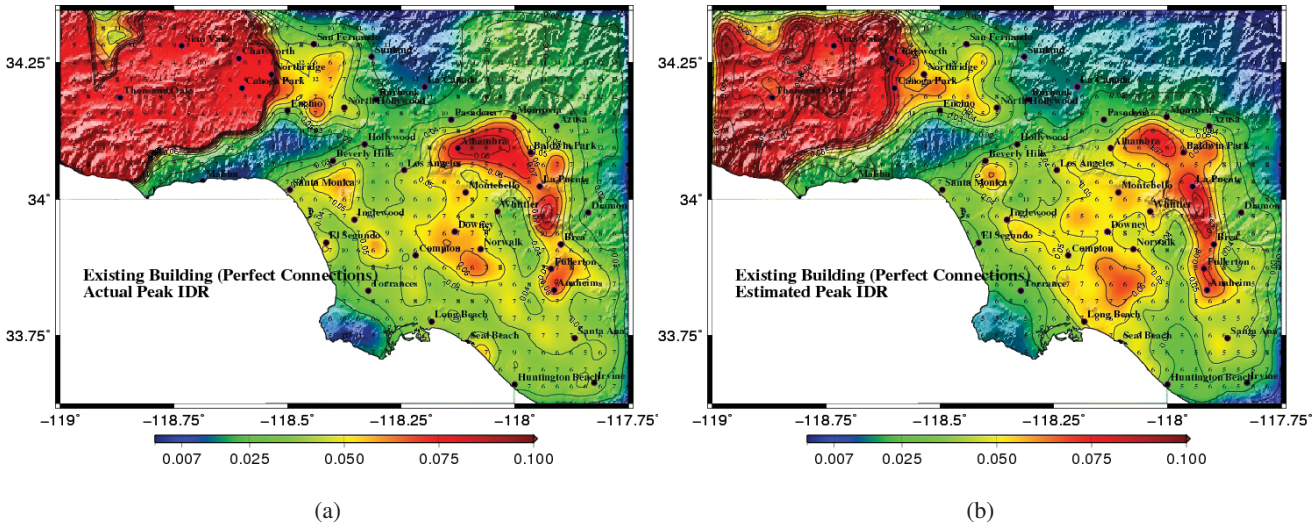

Figure 10: (a) Map of peak transient IDR in Building 1 (perfect connections) computed using synthetic 3-component waveforms at 636 sites from the 1857-like San Andreas earthquake simulation (b) The corresponding map of estimated IDR using the structural responses under idealized wave-train representation of the horizontal components of the synthetic motion.

```
INITIATE T = 0.50s:0.25s:6.00s
INITIATE V = 0.125m/s:0.125m/s:2.500m/s
INITIATE N = 1:1:5
GENERATE IDEALIZED WAVES USING ALL [Ti, Vj, Nk] COMBINATIONS

FOR EACH Ni, FIND THE [To, Vo] COMBINATION WITH THE LEAST ABSOLUTE DEVIATION BETWEEN
THE IDEALIZED WAVE AND EACH HORIZONTAL COMPONENT OF THE GROUND MOTION RECORD

FOR EACH [Ti, Vi, Ni] COMBINATION (i=1:5), DETERMINE PEAK IDR & LOCATION FROM STRUCTURAL
RESPONSE DATABASE. DO THIS STEP FOR BOTH HORIZONTAL COMPONENTS.  THE ABSOLUTE MAXIMUM OF
ALL THESE IDRs IS THE CURRENT ESTIMATE OF THE PEAK TRANSIENT IDR

FOR EACH i=1:5
  FOR EACH j=1:i−1
    IF 0.125 < (Vj−Vi) < 0.500
      Vi (CORR) = (i*Vi−j*Vj)/(i−j)
      PKIDR1 = PKIDR(Tj, Vj, Nj)
      LOC1 = LOC(Tj, Vj, Nj)
      PKIDR2 = PKIDR(Ti, Vi (CORR), Ni−Nj)
      LOC2 = LOC(Ti, Vi (CORR), Ni−Nj)
      IF LOC1==LOC2
        CURRENT ESTIMATE OF PEAK IDR = MAX(CURRENT ESTIMATE OF PEAK IDR, PKIDR1+PKIDR2)
```

Figure 11: Pseudocode for the rapid damage estimation procedure.

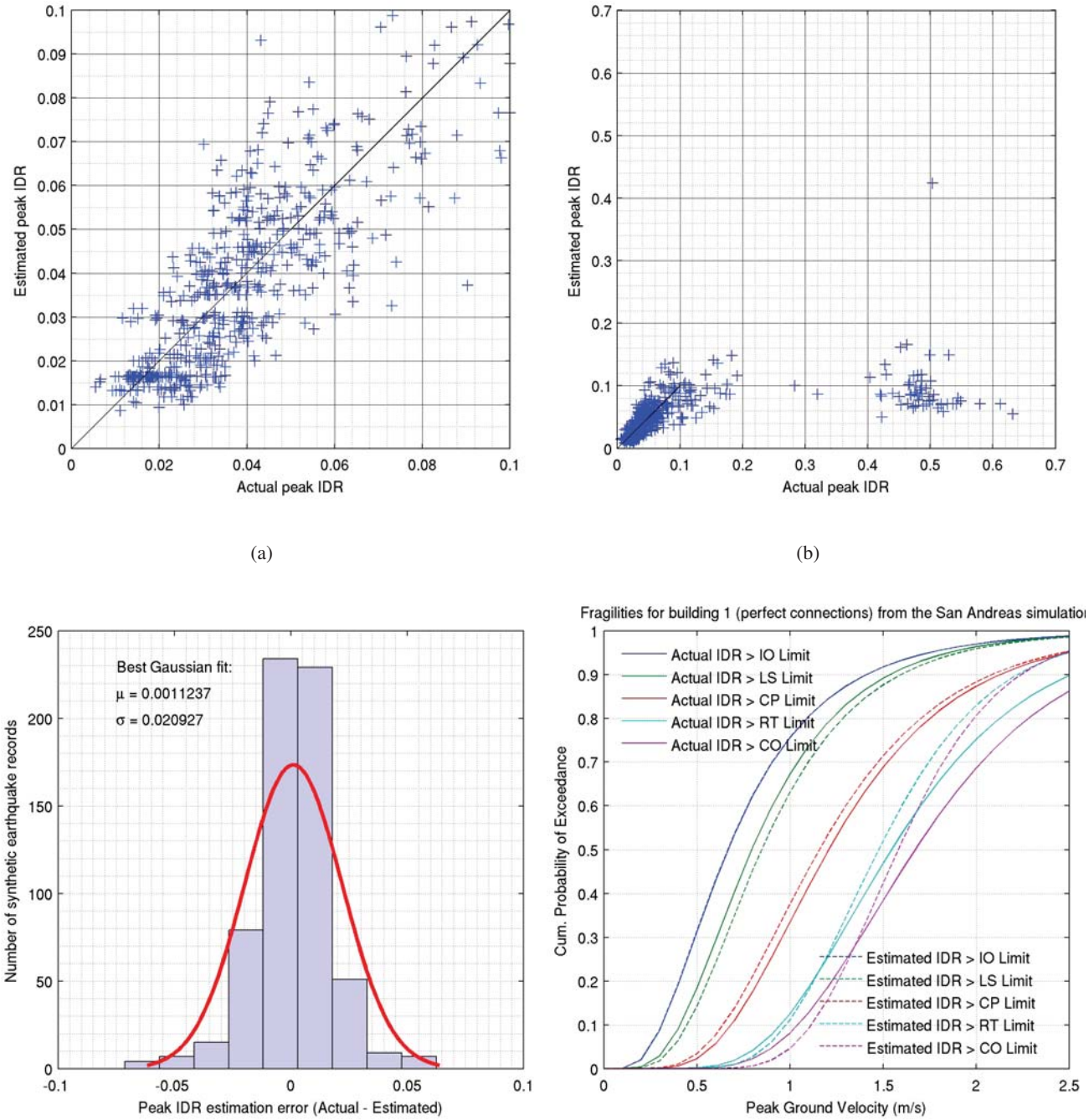

Figure 12: (a) and (b) The values of estimated and actual peak IDRs at each of the 636 southern Californian sites from Figure 10 plotted against each other. (c) Histogram of the estimation error and the best Gaussian fit. (d) Comparison of fragilities determined using computed responses in Figure 10(a) and the estimated responses in Figure 10(b).

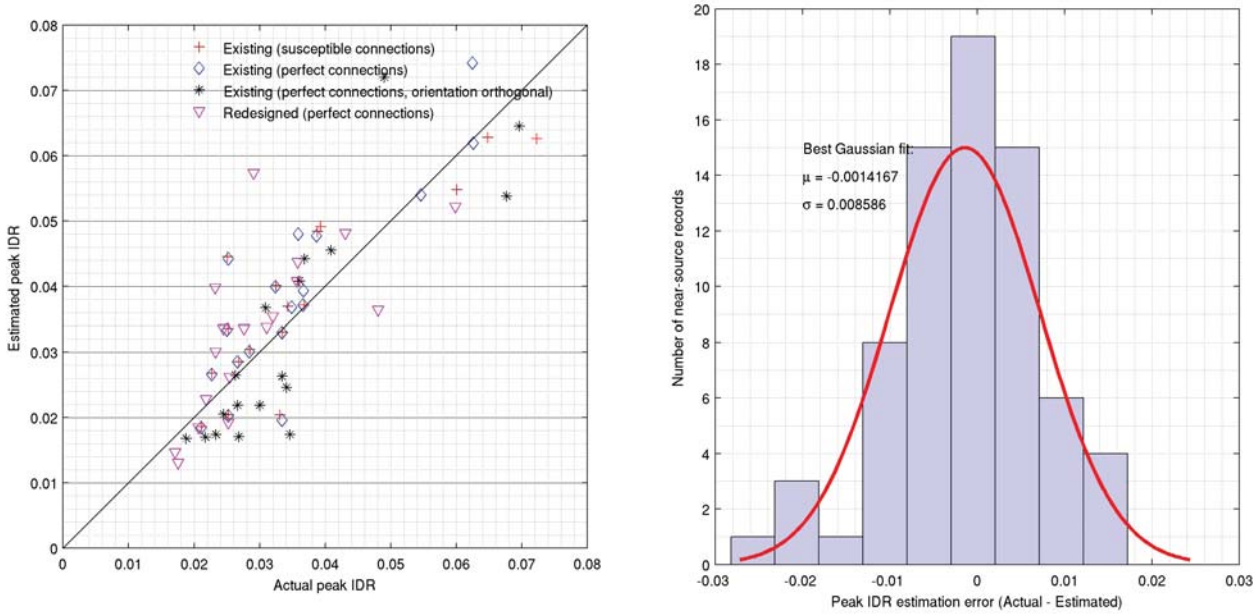

(a) (b)

Figure 13: (a) Peak transient IDR computed using all near-source records plotted against that computed using not the best-fit idealized 1-cycle waves as in Figure 8, but the rapid estimation methodology adopted for the San Andreas case: All buildings. The diagonal line represents identical results from the two analyses. (b) Histogram of the error in determining the peak transient IDR from the idealized waveform representation as opposed to the actual record. The best-fit Gaussian is also shown.

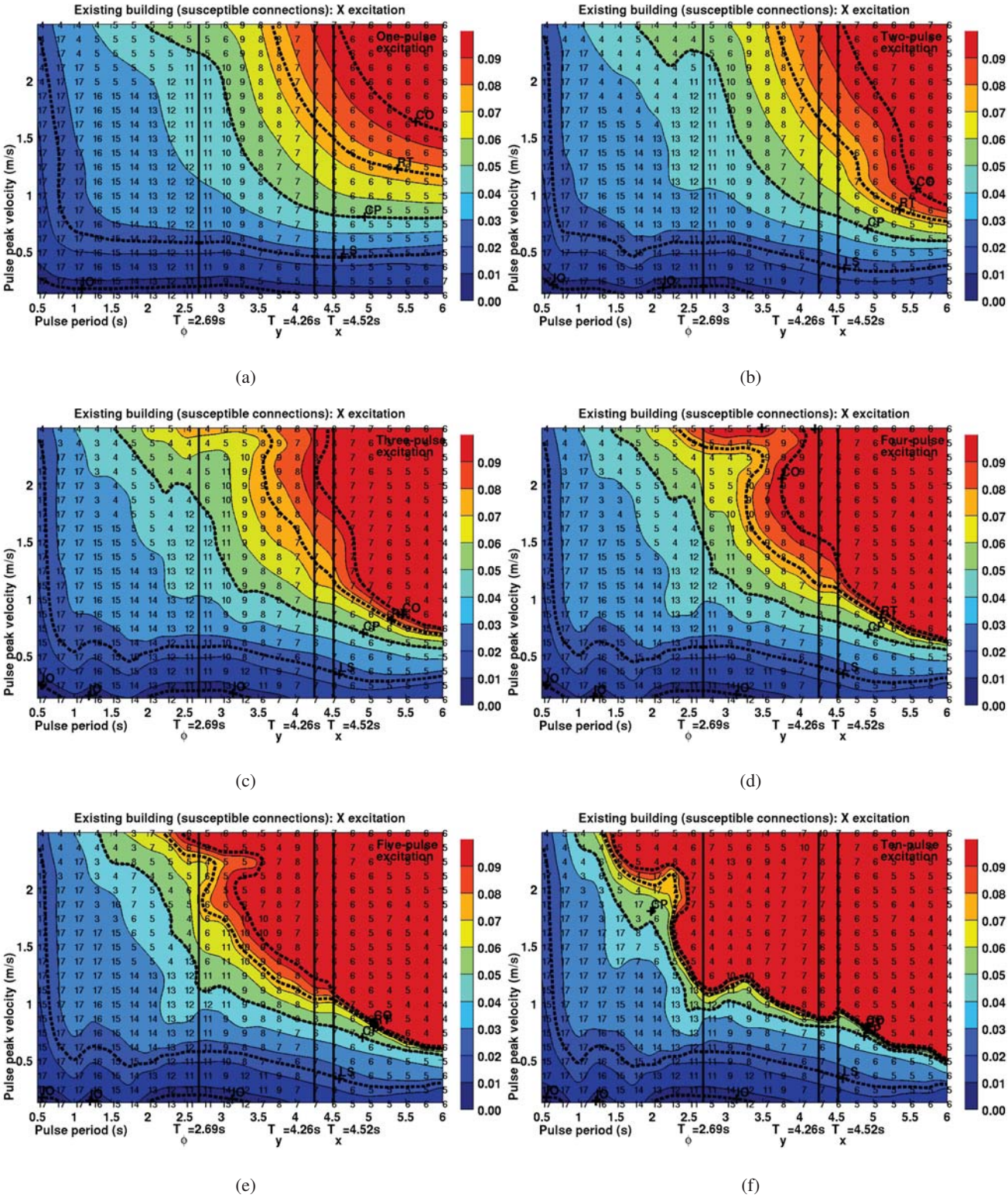

Figure 14: Peak transient IDR maps for Building 1 (susceptible connections) as a function of idealized ground excitation wave train parameters, period, PGV, and number of cycles. The one-component ground motion is applied in the building X direction. Contours corresponding to empirical performance levels of "Immediately Occupiable (IO)", "Life Safe (LS), "Collapse Prevented (CP)", "Red-Tagged (RT)", "Collapsed (CO)", are shown in bold font. The principal direction building fundamental periods are indicated for reference.

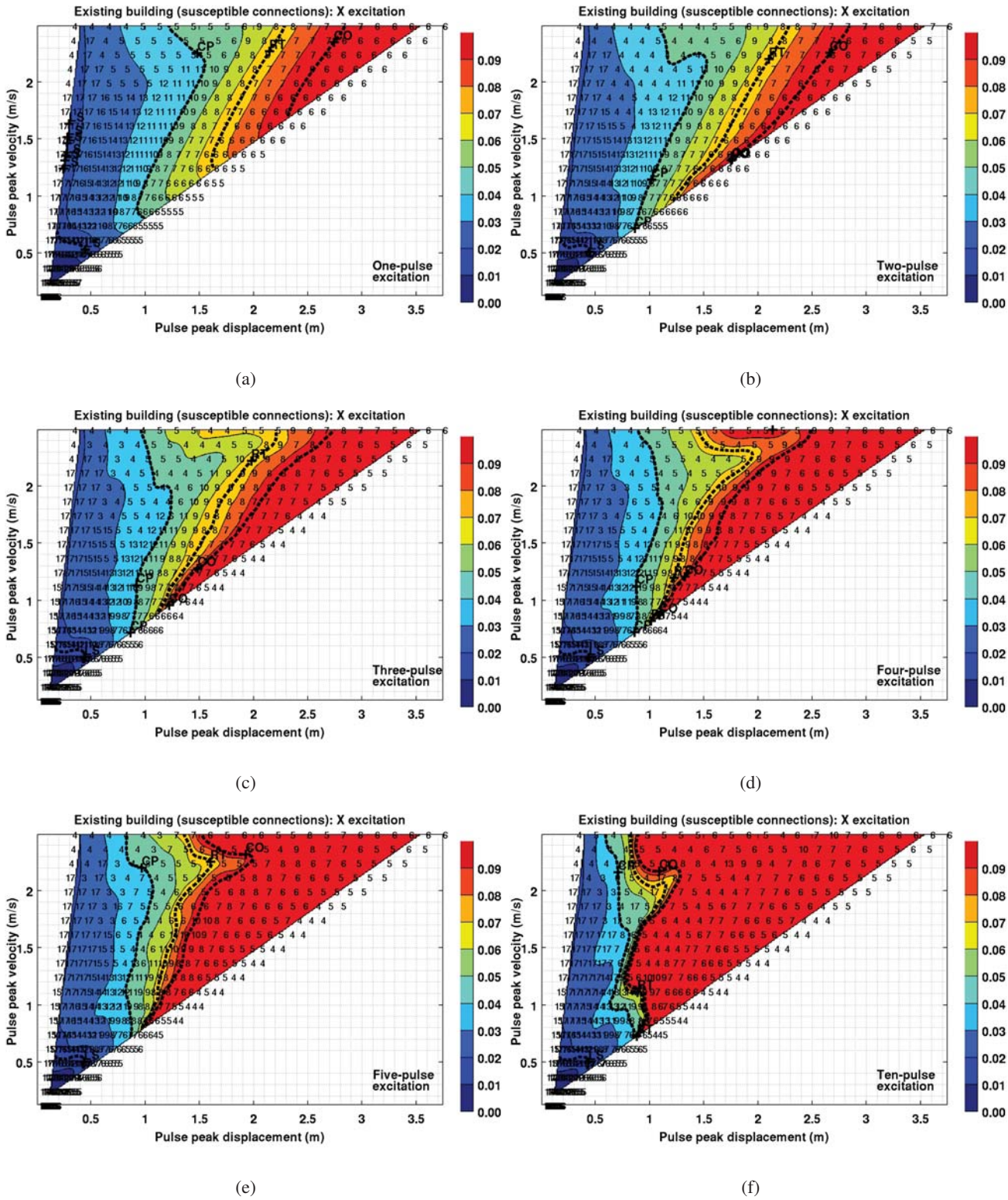

Figure 15: The peak transient IDR maps for Building 1 (susceptible connections) from Figure 14 transformed to the PGD-PGV plane. Contours corresponding to the empirical IO, LS, CP, RT, and CO performance levels are also transformed and shown in bold font.

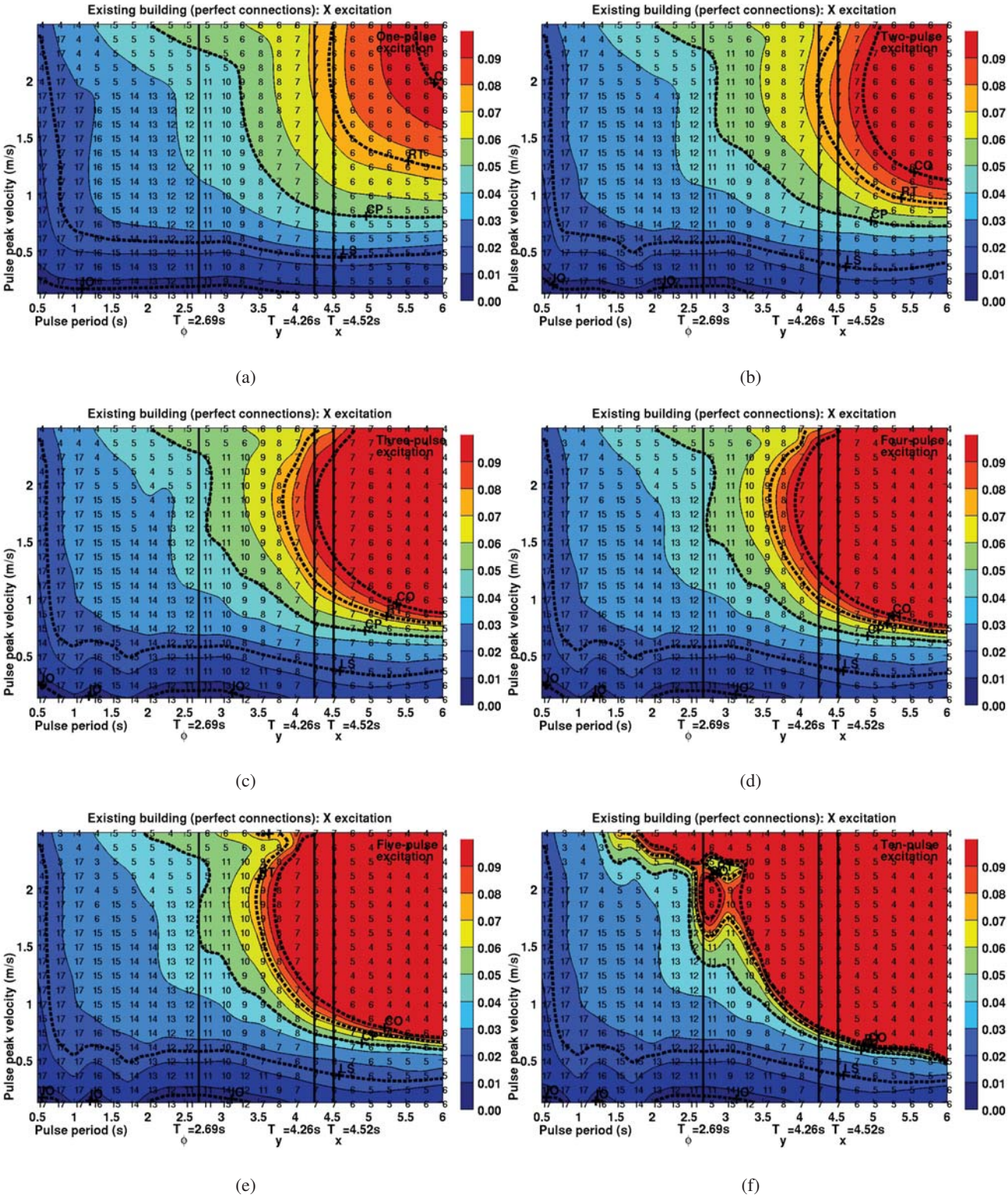

Figure 16: Peak transient IDR maps for Building 1 (perfect connections) as a function of idealized ground excitation wave train parameters, period, PGV, and number of cycles. The one-component ground motion is applied in the building X direction. Contours corresponding to the empirical IO, LS, CP, RT, and CO performance levels are shown in bold font. The principal direction building fundamental periods are indicated for reference.

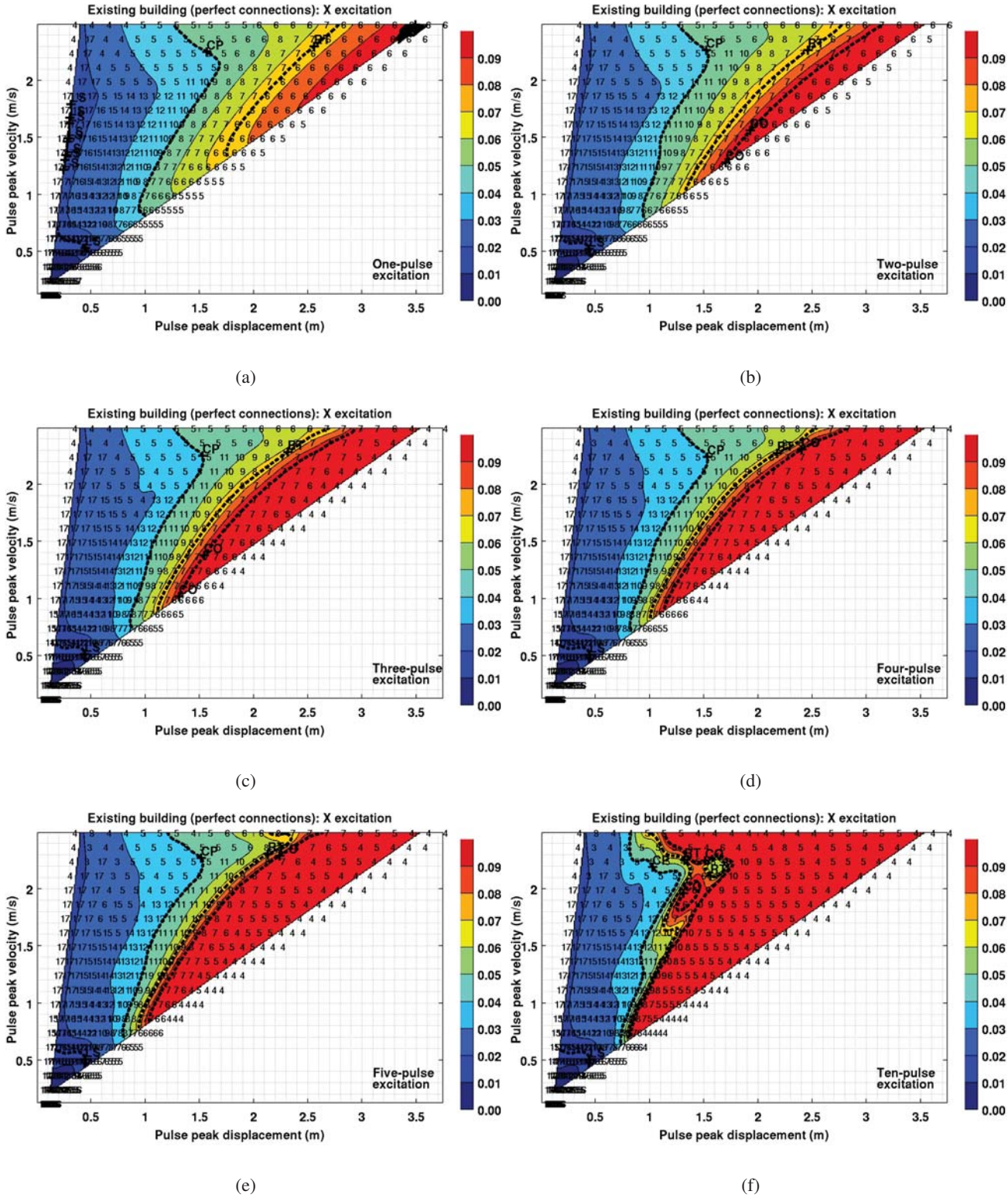

Figure 17: The peak transient IDR maps for Building 1 (perfect connections) from Figure 16 transformed to the PGD-PGV plane. Contours corresponding to the empirical IO, LS, CP, RT, and CO performance levels are also transformed and shown in bold font.

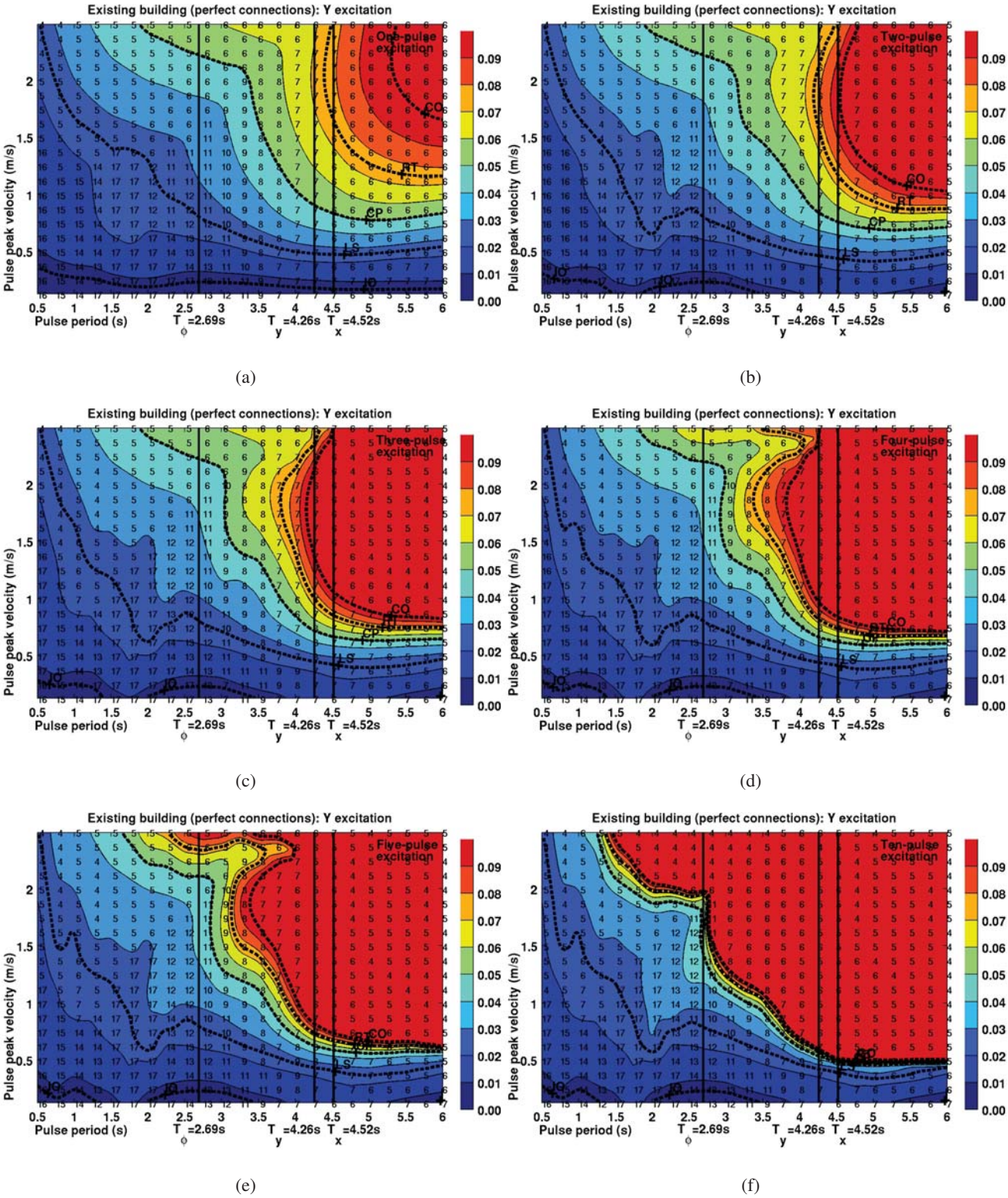

Figure 18: Peak transient IDR maps for Building 1 (perfect connections) as a function of idealized ground excitation wave train parameters, period, PGV, and number of cycles. The one-component ground motion is applied in the building Y direction. Contours corresponding to the empirical IO, LS, CP, RT, and CO performance levels are shown in bold font. The principal direction building fundamental periods are indicated for reference.

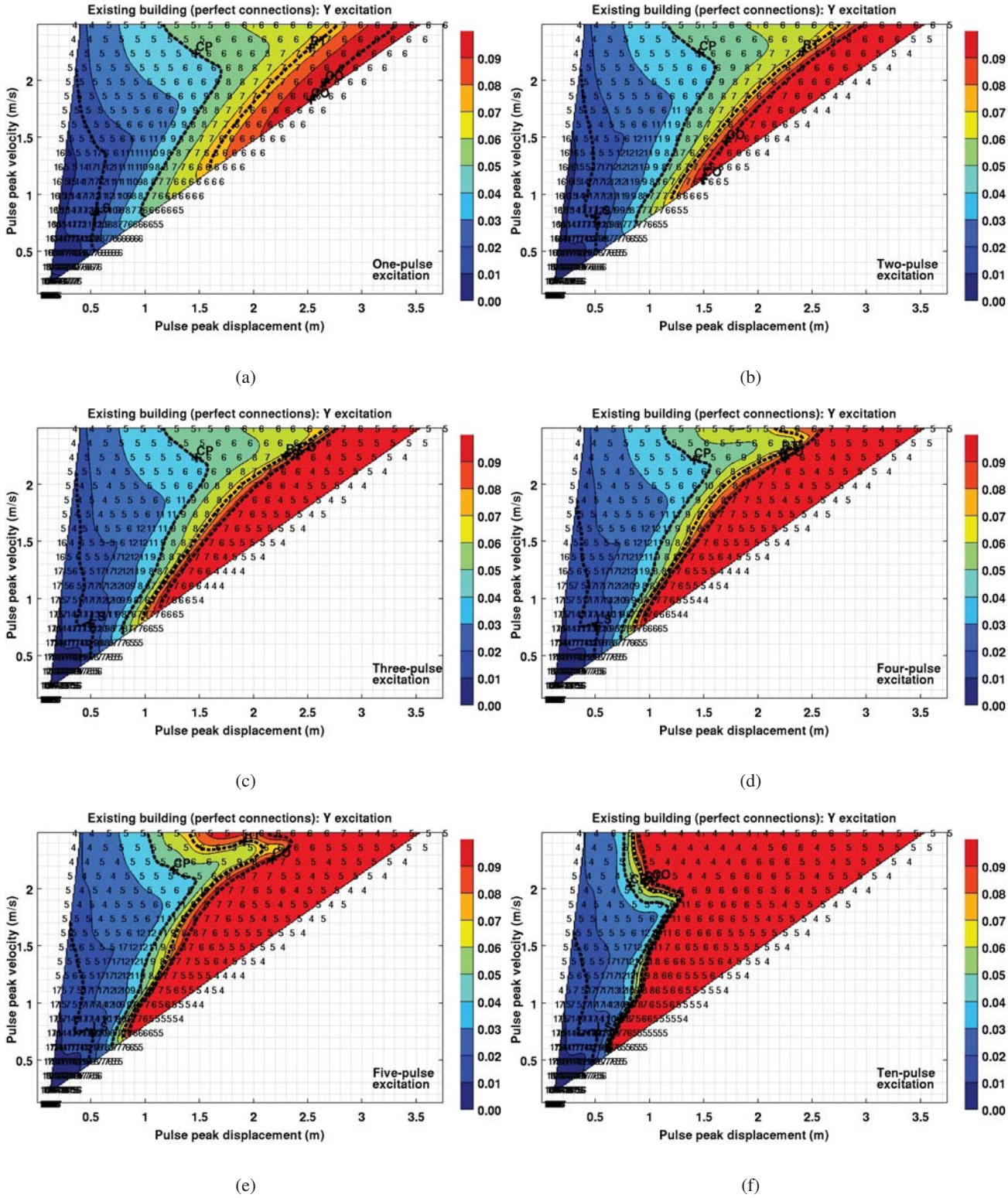

Figure 19: The peak transient IDR maps for Building 1 (perfect connections) from Figure 18 transformed to the PGD-PGV plane. Contours corresponding to the empirical IO, LS, CP, RT, and CO performance levels are also transformed and shown in bold font.

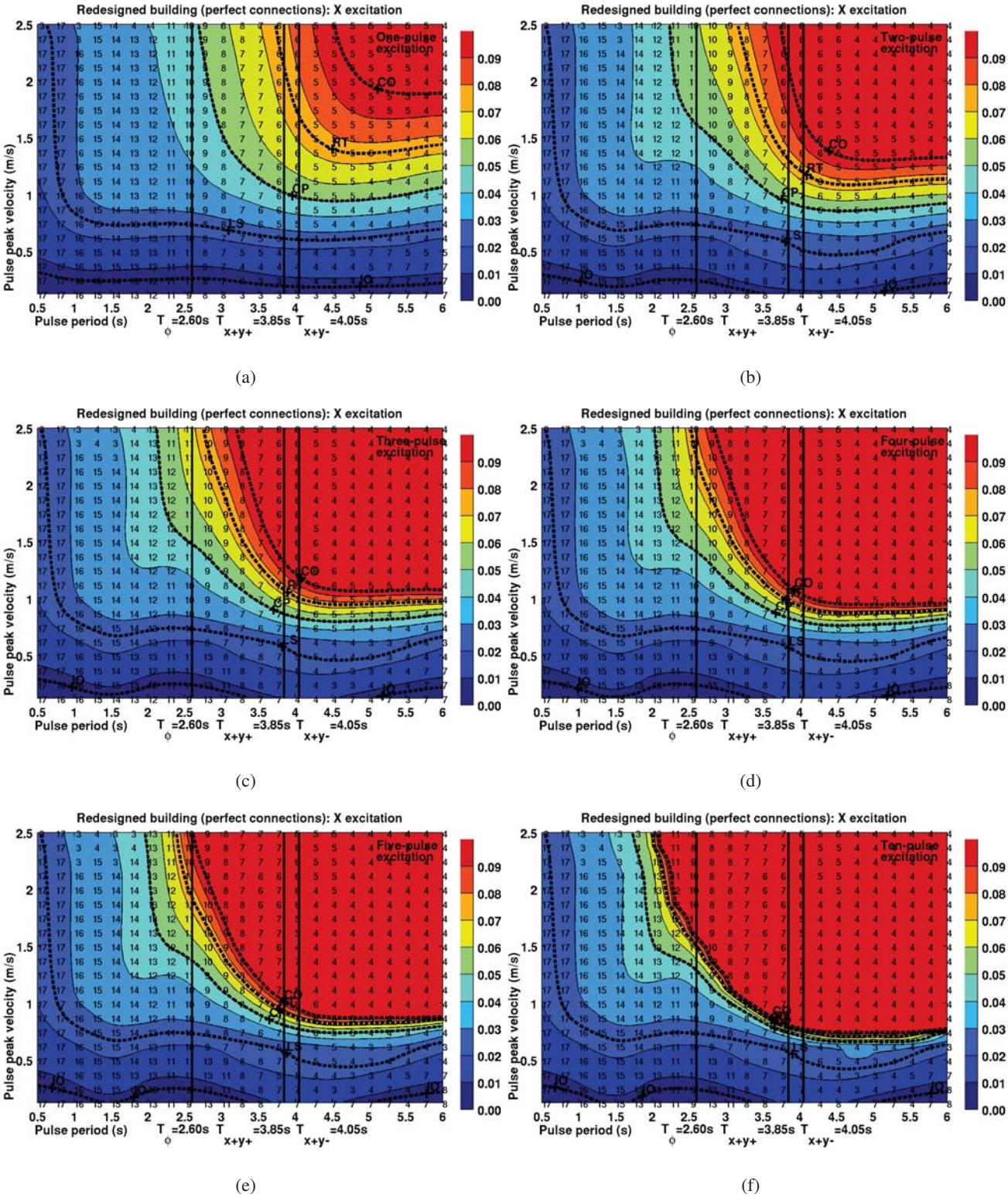

Figure 20: Peak transient IDR maps for Building 2 (perfect connections) as a function of idealized ground excitation wave train parameters, period, PGV, and number of cycles. The one-component ground motion is applied in the building X direction. Contours corresponding to the empirical IO, LS, CP, RT, and CO performance levels are shown in bold font. The principal direction building fundamental periods are indicated for reference.

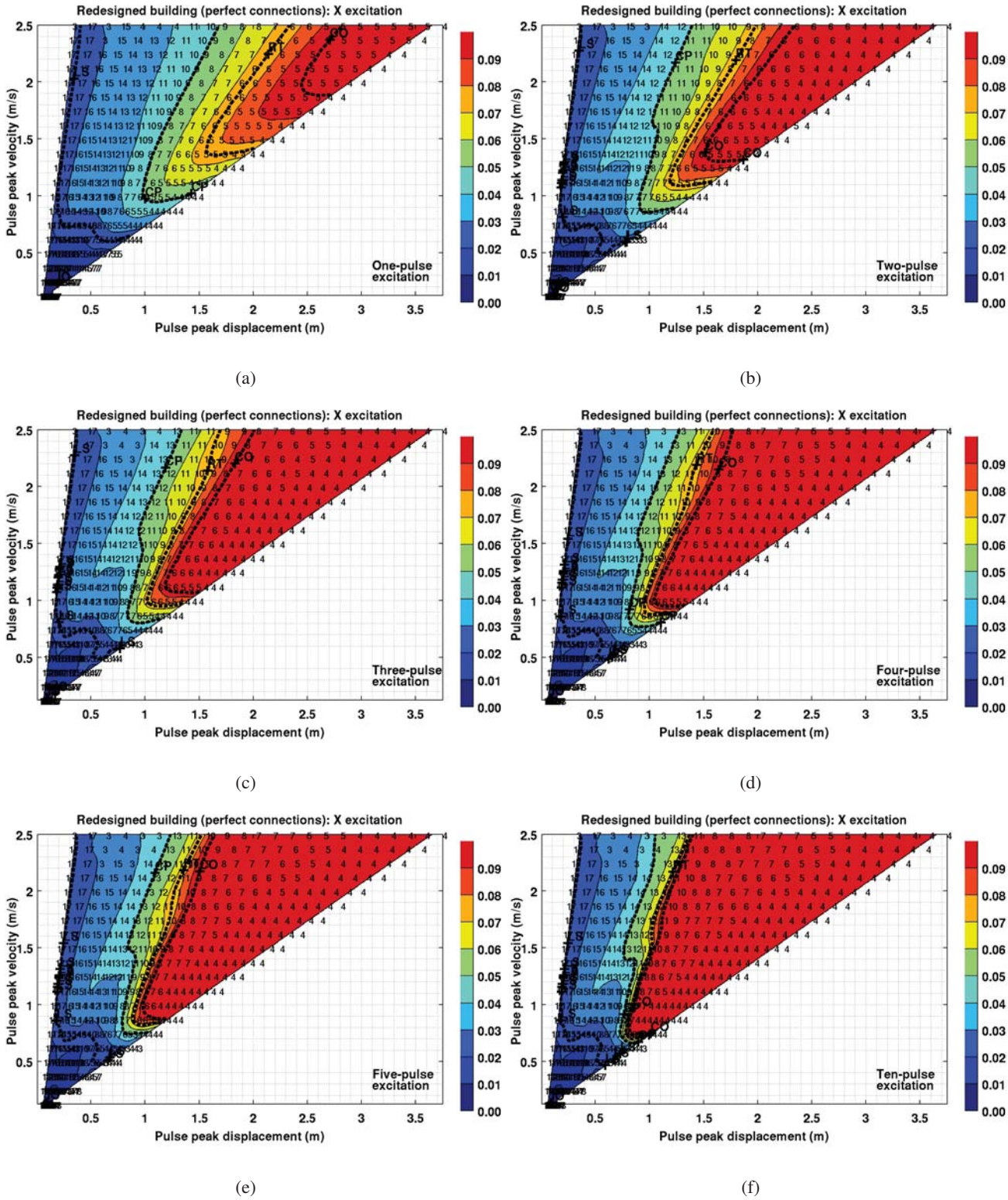

Figure 21: The peak transient IDR maps for Building 1 (perfect connections) from Figure 20 transformed to the PGD-PGV plane. Contours corresponding to the empirical IO, LS, CP, RT, and CO performance levels are shown in bold font.